npj Computational Materials

www.nature.com/npjcompumats

ARTICLE OPEN

The exotically stoichiometric compounds in Al–S system under high pressure

Sen Shao[1], Wenji Zhu[1], Jian Lv[1*], Yanchao Wang[1*], Yue Chen[2] and Yanming Ma[1,3]

Aluminum and sulfur, as abundant elements in earth, only form Al_2S_3 in nature at ambient pressure. It has been realized that the stoichiometry of compounds may change under high pressure, which is crucial in the discovery of novel materials. In this work, we systematically perform structure search for Al–S system under pressure. Four binary compounds of Al–S with exotic stoichiometries of AlS, Al_2S, Al_3S_4, and AlS_2 are found at high pressure and show exciting physical properties. In particular, Al_3S_4 becomes a superconductor with a predicted superconducting transition temperature T_c of 20.9 K at 100 GPa, while the pressure-induced Al_2S becomes an electride, where the valence electrons of aluminum strongly localize in the interstices, acting as anions, at a pressure of 70 GPa. This work provides a viable direction for further experimental study of the properties of Al–S system.

npj Computational Materials (2020)6:11 ; https://doi.org/10.1038/s41524-020-0278-9

INTRODUCTION

Aluminum and sulfur are among abundant elements in earth and have broad applications in industry.[1,2] For instance, they have been used extensively in batteries for high energy density and acceptable voltage in recent years.[3,4] As aluminum and sulfur have +3 and −2 oxidation states, respectively, only Al_2S_3 has been observed in nature. The stable phase of Al_2S_3 is in $P6_1$ arrangement (α-phase), with a wide bandgap at ambient pressure,[5–7] and has been used extensively for electronic devices (e.g., aluminum-based sulfide solid-state battery[8]). A recent investigation indicates that Al–S battery is a promising candidate for use in high-performance low-cost energy-storage systems.[9] The phase transitions of Al_2S_3 under pressure have been studied extensively in experiments, and several Al_2S_3 with different polymorphisms have been proposed, such as β-Al_2S_3[6,10] and γ-Al_2S_3.[6] Some defect structures of Al_2S_3, including tetragonal defect spinel phase, are synthesized under high pressures and temperatures.[11]

It is well known that pressure is considered as a powerful tool to rearrange electrons, modify chemical bonding, and create new exotic materials.[12–17] In this context, binary sulfides are typically systems showing intriguing structure and properties under compression, which continues to surprise us. For example, hydrothion with distinctive odor of rotten eggs is the only stable compound in H–S system at ambient conditions. Several novel compounds have been predicted under pressures, such as H_3S, HS_2, H_2S_3, H_3S_2, H_4S_3, and H_5S_2.[18,19] A breakthrough finding in H–S system is the observation of a remarkably high superconducting T_c value of 203 K under pressure.[20] Similarly, a great deal of novel compounds and chemical properties have been found in Li–S system under high pressure.[21] In particular, a new compound Li_3S has been found to be an electride with a high T_c value. Furthermore, when sulfur is mixed with the IIA group element Be in stoichiometry of 1:1, a modulated structure occurs, which is unusual for such simple binary compounds.[22] The intriguing structures and properties of group IA and IIA sulfides motivate us to further investigate binary mixture between S and group IIIA element Al under pressures.

Herein, we systematically search the crystal structures of different stoichiometric Al–S systems. Several new compounds of AlS, Al_2S, Al_3S_4, and AlS_2 are found to be stable under pressures, which show intriguing properties. In particular, we find several potential superconductors, such as Al_3S_4 and AlS, and a new electride Al_2S, where the valence electrons of aluminum strongly localize in the interstices, acting as anions, at high pressure.

RESULTS

We perform an extensive search for crystal structures of Al_xS ($x = 1/3$, 2/5, 1/2, 2/3, 3/4, and 1–3) at 50, 100, 150, and 200 GPa with maximum simulation cells up to 4 formula units (f.u.) for each fixed composition by using an in-house-developed Crystal structure AnaLYsis by Particle Swarm Optimization (CALYPSO) methodology.[23,24] All the candidate structures are relaxed by Vienna ab initio Simulation Package (VASP) code,[25] and the thermodynamic stabilities of Al–S system with variable stoichiometries are systematically investigated by means of calculating the formation enthalpies relative to Al and S at corresponding pressure. The enthalpy of formation per atom is calculated by using the following formula:

$$\Delta H = \left[H(Al_xS_y) - xH(Al) - yH(S)\right]/(x+y)$$

Convex hull data at 0 K under different pressures is summarized in Fig. 1a. The compounds located on the convex hull are stable. Figure 1b shows the stable pressure ranges of different phases.

At ambient conditions, only Al_2S_3 compound is stable. Our results (Fig. 1) show that it is still the most stable compound on the convex hull at 50 GPa. However, Al_2S_3 decomposes into AlS_2 and Al_3S_4 under further compression, and becomes thermodynamically stable again at 140 GPa. Pressure has enormous influence on crystal structures and energies by altering interatomic distances and chemical bonding. Some unexpected stoichiometric compounds are found to be stable under pressure. Al_3S_4 and AlS are the most energetically stable compounds at 100 and 150 GPa, respectively. Al_2S and AlS_2 also locate on the convex hull, which implies that these compounds are also stable under pressure, but their formation enthalpies are slightly higher than others. The

[1]State Key Laboratory of Superhard Materials & International Center for Computational Method and Software, Jilin University, Changchun 130012, China. [2]Department of Mechanical Engineering, The University of Hong Kong, Pokfulam Road, Hong Kong, Hong Kong SAR. [3]International Center of Future Science, Jilin University, Changchun 130012, China. *email: lvjian@jlu.edu.cn; wyc@calypso.cn

other four predicted compounds (Al_2S_5, Al_5S_2, Al_3S, and AlS_3) are located above the convex hull, implying that they are unstable.

Al_2S_3

Figure 1 shows that Al_2S_3 compound exhibits various crystal structures under pressure. In order to identify the sequence of phase transformation for Al_2S_3, the structures synthesized in experiments must be taken into consideration. Several crystalline forms of Al_2S_3 are known, but not all of them have been strictly characterized, and three structures that have detailed lattice parameters, are considered here.[6,7,11] The enthalpies per atom of all phases predicted and synthesized for Al_2S_3 are shown in Fig. S1. Al_2S_3 is in a hexagonal $P6_1$ atomic arrangement (α-phase) at atmospheric pressure, in which the Al atoms are 4 or 5 coordinated to S atoms (Fig. S2). Under further compression, this structure transforms to the $I4_1/amd$ (δ phase) at ~0.4 GPa and then to R-3c phases (γ-phase) at 6 GPa, where the coordination number of Al increases to six. Our predicted $Pbcn$, $P6_3$/mcm, $P4/mbm$, and P-1 phases (Table S1) are stable in pressure ranges of 25–70, 70–95, 140–170, and above 170 GPa, respectively. The coordination number of Al in $Pbcn$ and $P6_3$/mcm phases remains six, while it increases to eight in the $P4/mbm$ and P-1 phases. It should be pointed out that the increase in coordination number is a common phenomenon for materials at high pressures.

To understand the nature of the chemical bond of Al_2S_3, the electron localization function (ELF)[26] and Crystal Orbital Hamilton Population (COHP),[27,28] as well as the integrated COHP (ICOHP) up to Fermi level, are calculated (Table S2). Here, we take the $P4/mbm$ phase as an example (Fig. 2a). The calculation of ELF on the (2 3 1)

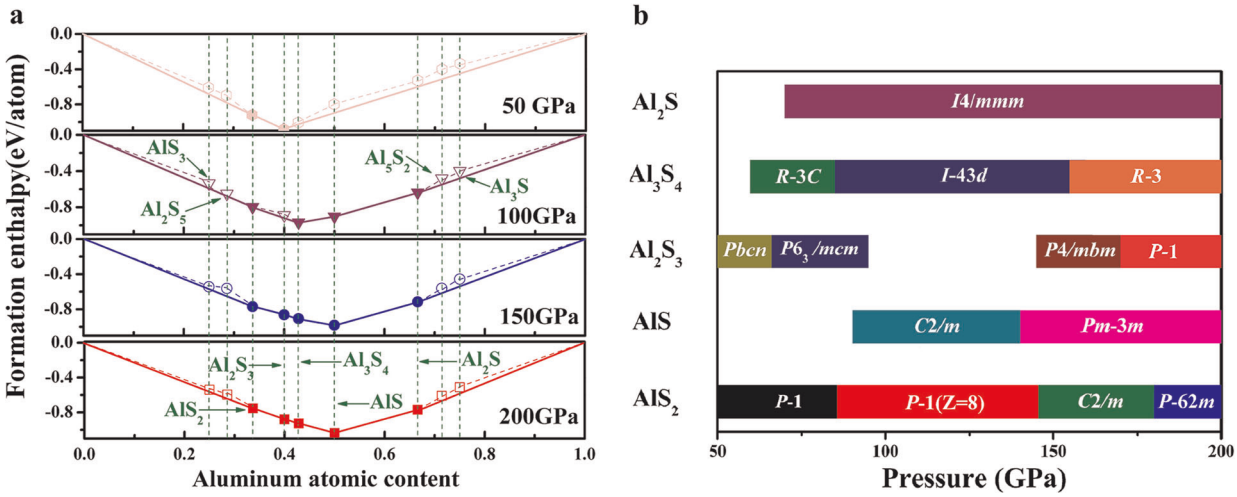

Fig. 1 Thermodynamic stabilities and stable pressure ranges of Al_xS_y compounds. a Thermodynamic stabilities of various Al_xS_y compounds with respect to elements Al and S at 0 K and different pressures. The energetically stable phases are shown using solid symbols connected by solid lines on the convex hull. **b** Pressure ranges in which the corresponding phases of different Al–S compounds are thermodynamically stable.

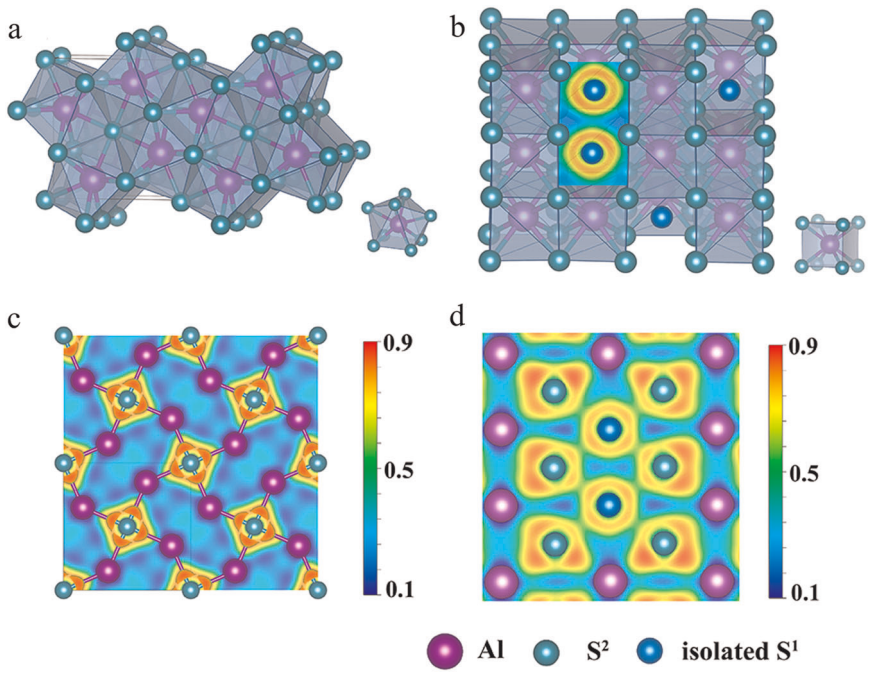

Fig. 2 Crystal structures and bonding properties of Al_2S_3. a $P4/mbm$ structure at 150 GPa. **b** P-1 structure at 200 GPa with unique isolated S^1 sulfur atoms shown in blue. **c** Calculated ELF of the $P4/mbm$ phase on (0 0 1) plane at 150 GPa. **d** ELF calculated on the (2 3 1) plane of the P-1 phase at 200 GPa.

plane at 150 GPa is shown in Fig. 2c. The ELF has strong directionality from S to Al, and the value of ICOHP of Al–S bond is −3.33 eV similar to that of S–S bond (−2.81 eV) in solid S (*R*-3*m*) at the same pressure. The results indicate the existence of covalent bonds between S and Al.

At 200 GPa, Al_2S_3 is stable in triclinic *P*-1 structure, which is mainly composed of S-sharing eightfold AlS_8 hexahedrons, whereas several unique isolated sulfur atoms (isolated sulfur atom in blue named S^1, the others named S^2) exist, appearing in pairs, between these hexahedrons (see Fig. 2b). The ELF is calculated (Fig. 2d) at 200 GPa, which reveals that electrons are mainly localized between Al and S^2. The calculated ICOHP value (−2.42 eV) of Al–S^2 at 200 GPa is similar to that of S–S bonds in solid S (−2.90 eV) at the same pressure, suggesting that Al and S^2 form covalent bonds. The distance between isolated S^1 and Al is 2.51 Å, which is much longer than the bond length of Al–S at ambient conditions. In addition, the values of ICOHP for Al–S^1 pairs (−1.07 eV) and S^1–S^2 pairs (−1.51 eV), have been shown, indicating a weak interaction in Al–S^1 and S^1–S^2 pairs.

Al_3S_4

Al_3S_4 is stable in a crystal structure with *R*-3*c* symmetry above 60 GPa. It is significantly different from other compounds that aluminum in AlS_7 coordination is found for the first time in Al–S system. Under further compression, this compound transforms into a cubic *I*-43*d* phase, having similar structural features to lanthanum chalcogenides with the same stoichiometry.[29] At 100 GPa, the cubic *I*-43*d* Al_3S_4 becomes the most energetically stable in all Al–S compounds. The calculated ELF (Fig. 3a) and the average value of ICOHP (−2.85 eV) for Al–S pairs in *I*-43*d* structure at 100 GPa, which is comparable to that for S–S pairs (−2.59 eV) in solid S at the same pressure, reveal the presence of covalent bonds between Al and S. The cubic *I*-43*d* phase is overtaken by *R*-3 phase of Al_3S_4 above 160 GPa. The trigonal *R*-3 phase has some similar characteristics to triclinic Al_2S_3. An isolated sulfur atom S^1 (Fig. 3b) locates in the center of the lattice, while others (S^2) surround aluminum forming AlS_8 hexahedrons linked by means of sharing edges with adjacent AlS_8 hexahedrons.

All the three phases are metallic having a sizable DOS at Fermi level under the entire stable pressure range. Therefore, we estimated superconducting transition temperature (T_c) of *R*-3*c*, *I*-43*d*, and *R*-3 phases through electron–phonon coupling (EPC) calculations at 60, 100, and 200 GPa, respectively. Here, we take the *I*-43*d* phase as an example. Figure 3d shows the EPC spectral function $\alpha^2F(w)$, the integral λ, and the projected phonon density of states (PHDOS) for cubic phase Al_3S_4. It illustrates that Al and S elements have the comparable contributions to the superconductivity. The resultant T_c value is 17.7–20.9 K ($\mu^* = 0.10$~0.13) at 100 GPa. The calculated T_c values for *R*-3*c* and *R*-3 are 0 and 9.97 K at 60 and 200 GPa, respectively.

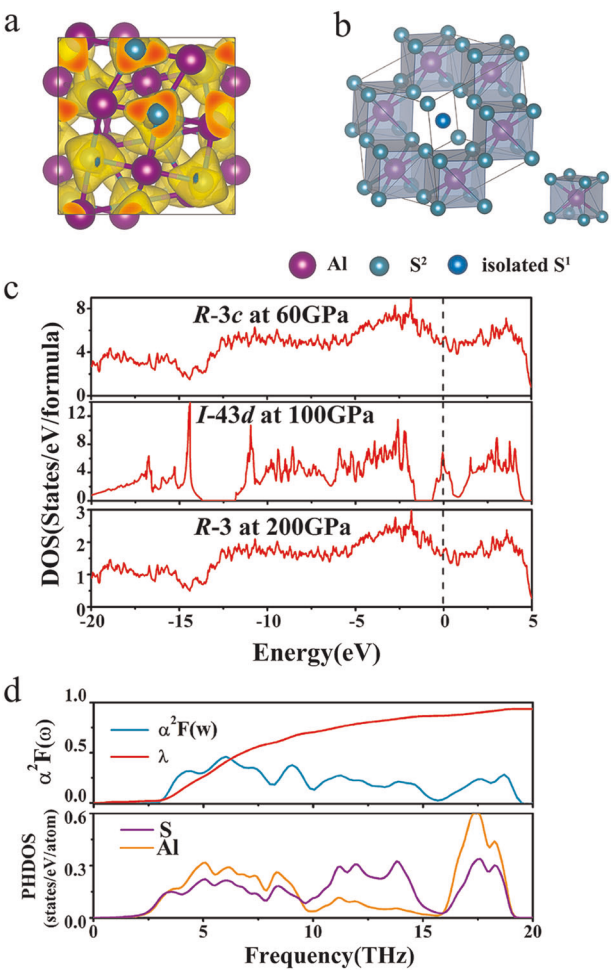

Fig. 3 Crystal structures and properties of Al_3S_4. **a** Calculated ELF of cubic *I*-43*d* Al_3S_4 with an isosurface value of 0.75. **b** Crystal structure of *R*-3 Al_3S_4. **c** Plots of DOS for the *R*-3*c*, *I*-43*d*, and *R*-3 phases. **d** The projected phonon density of states (lower panel), Eliashberg EPC spectral function $\alpha^2F(\omega)$, and its integral $\lambda(\omega)$ (upper panel) of Al_3S_4 (*I*-43*d*) at 100 GPa.

AlS

Two crystal structures of AlS with *C*2/*m* (Fig. 4a) and *Pm*-3*m* (Fig. 4b) symmetries are discovered in our calculations. As shown in Fig. 1b, *C*2/*m* structure is stable above 90 GPa and transforms into cubic *Pm*-3*m* structure when the pressure reaches 150 GPa.

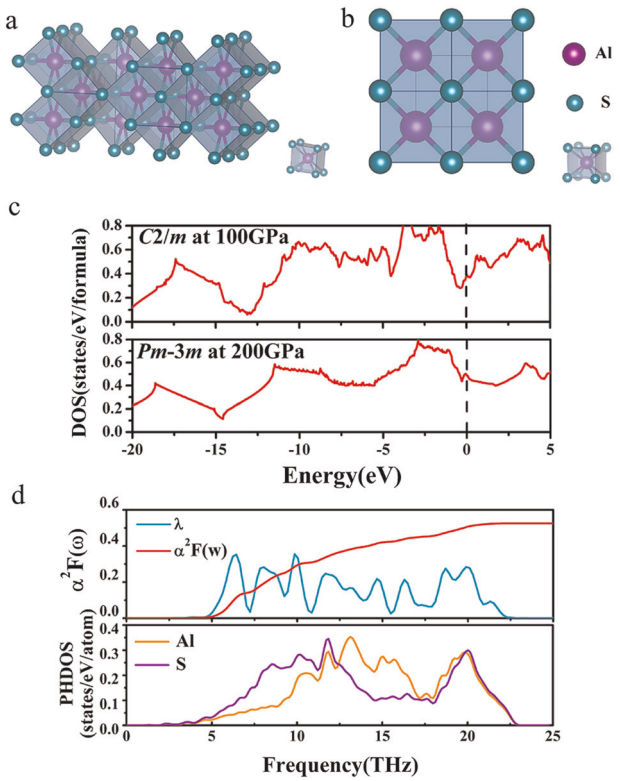

Fig. 4 Crystal structures and properties of AlS. The *C*2/*m* (**a**) and *Pm*-3*m* (**b**) phases of AlS. **c** DOS of the *C*2/*m* and *Pm*-3*m* phases. **d** The projected phonon density of states (lower panel), Eliashberg EPC spectral function $\alpha^2F(\omega)$, and its integral $\lambda(\omega)$ (upper panel) of AlS (*Pm*-3*m*) at 200 GPa.

Both phases of AlS show metallic features (Fig. 4c). Here, we perform EPC calculations for the *Pm*-3*m* structure at 200 GPa. Figure 4d reveals that Al and S elements have comparable contributions to the superconductivity, which mainly originates from the polar covalent bonds. At $\mu^* = 0.10$, the resultant T_c value is 7.6 K, being much lower than that of Al_3S_4 at 100 GPa.

Al_2S

For Al-rich stoichiometries, we find that Al_2S with *I*4/*mmm* symmetry is stable in the pressure range of 70–200 GPa. The crystal structure of Al_2S composed of interlaced [Al_2S] layers is shown in Fig. 5a. This tetragonal crystal structure has similar layered characteristics to Ca_2N electride.[30–32] ELF plot of Al_2S with an isosurface value of 0.69 at 100 GPa (Fig. 5b) indicates the existence of localized electrons in the interstices instead of locating at the center of the Al–Al bonds, suggesting the formation of an electride. We calculated the Bader charges[33] for the Al_2S (Table S3). Besides six electron density maximum points located at the centers of Al and S atoms, we found that the extra four electron density maximum points are located at the positions of interstitial electrons, which can be seen as interstitial quasi-atoms (ISQs).[34] So, the Al_2S can be regarded as an electride.

Electride is a class of extraordinary compounds with valence electrons occupying interstices instead of being attached to atoms. These interstitial electrons can occupy shallow bands, leading to a dramatically reduced work function and large conductive properties. In known inorganic electrides,[17,35–39] it seems that alkali and alkaline earth metals, as well as their compounds, can easily form electrides, while aluminum compounds do not. Pickard and Needs found distinct "blobs" of interstitial electron density in aluminum crystal at 5 terapascals (TPa),[40] while alkali and alkaline earth metals can form electrides at a few hundred gigapascals (GPa).[41,42] So far, only a few aluminum-based electrides are found, including $[Ca_{24}Al_{28}O_{64}]^{4+}(e^-)_4$, Ba_4Al_5, Ba_7Al_{10}, and $Sr_3(AlSn)_2$.[43,44] However, the interstitial electrons of these electrides do not come from aluminum. Therefore, it is especially interesting that the Al_2S is found to be an electride, where interstitial electrons originate from aluminum, at a moderate pressure.

Figure 5c shows that Al_2S is metallic, and many bands with large dispersion traverse the Fermi level. The partial charge density (isosurface value of 0.0507 e/Å^3) within an energy window between −1 and 1 eV around Fermi level is shown in Fig. 5d. It is seen that the electrons are mainly located in the interlayers. Moreover, the value of linear-averaged electron density along the *z* direction has a maximum at the middle of the interstitial electronic plane, which suggests that the contributor to the bands within −1–1 eV around Fermi level basically derives from the interstitial electrons.

DISCUSSION

The variable stoichiometries in Al–S system have been systematically explored. Besides the well-known compound Al_2S_3, we identify four new stable compounds (Al_3S_4, AlS_2, Al_2S, and AlS) in the pressure range of 50–200 GPa. A number of aluminum sulfides become metals and are potential superconductors. A unique stoichiometry Al_3S_4 becomes stable at 60 GPa. This stoichiometry is known for the first time in aluminum chalcogenide, and it transforms into cubic *I*-43*d* geometry at 90 GPa, having a resembling structure and electronic characters with La_3S_4. This cubic structure is metallic with an estimated value of T_c around 20.7 K at 100 GPa. Al_2S is stable above 70 GPa, which is found to be an electride. It is especially interesting to find that the valence electrons of aluminum become localized in the crystal acting as

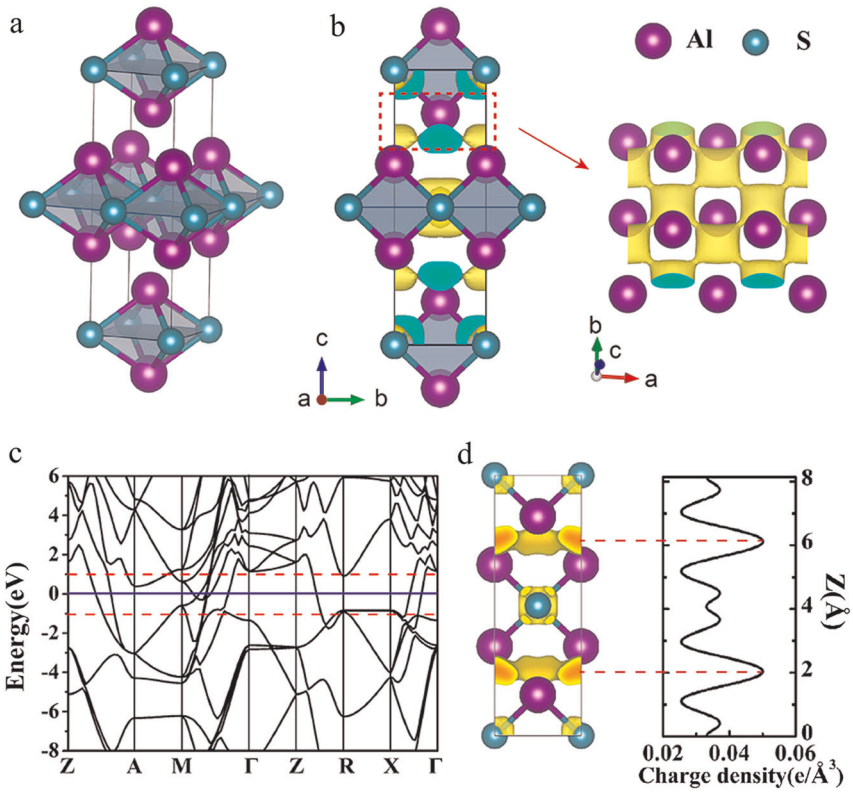

Fig. 5 Crystal structures and properties of *I*4/*mmm* Al_2S. **a** Crystal structure of *I*4/*mmm* Al_2S. **b** Calculated ELF of Al_2S with an isosurface value of 0.69 at 100 GPa. **c** Electronic band structure of Al_2S at 100 GPa. **d** Partial charge density (the isosurface value is 0.0507 e/Å^3) within 2 eV around the Fermi level in-between the two red dotted lines in the band structure (left panel), and the planar-averaged charge density along the *z* axis (right panel).

anions under pressure. AlS_2 is stable in the pressure range from 50 to 200 GPa. Above 150 GPa, AlS is found to be the most energetically stable compound with *Pm*-3*m* symmetry, and the estimated T_c value is 7.6 K at 200 GPa. This work provides guidelines for further experimental exploration of Al–S system under high pressure.

METHODS

The structure prediction for Al–S system is performed via a global minimum search of free energy surface by the swam intelligence-based CALYPSO method and its same name code.[23,24] This methodology is highly efficient to predict the stable structures, and benchmarked on various known systems.[16,45,46] The ab initio relaxations and electronic property calculations were performed based on density function theory[47,48] within the Perdew−Burke−Ernzerhof (PBE) of generalized gradient approximation (GGA),[49] as implemented in the Vienna ab initio Simulation Package (VASP) code.[25] The all-electron projector-augmented wave (PAW)[50] method has been adopted, with $3s^23p^1$ and $3s^23p^4$ treated as the valence electrons of Al and S atoms, respectively. A kinetic energy cutoff of 600 eV was used, and a dense *k*-point sampling of the Brillouin zone with a resolution of $2\pi \times 0.025$ Å^{-1} was adopted to ensure the enthalpy calculations converged within 1 meV/atom.

The phonon calculations were performed by using the finite displacement method as implemented in PHONOPY[51] code to verify the dynamical stability of structures. To analyze the interatomic interaction and chemical bonding, the crystal orbital Hamilton populations (COHP)[27,28] and the electron localization function (ELF)[26] were calculated using the LOBSTER[52] and VASP codes, respectively. The calculations of superconducting transition temperatures of the most stable structures were performed using the EPC module of the Quantum ESPRESSO code.[53] The kinetic energy cutoffs of plane-wave basis for Al_3S_4 and AlS were set to 85 Ry and 80 Ry, respectively, to ensure that the calculated energy converged within 1 meV/atom. The electron–phonon coupling (EPC) was calculated with a $7 \times 7 \times 7$ *q* mesh for Al_3S_4 and $8 \times 8 \times 8$ *q* mesh for AlS to ensure that the calculations are well converged.

DATA AVAILABILITY

All data generated or analyzed during this study are included in this published article (and its supplementary information files).

Received: 26 June 2019; Accepted: 15 January 2020;
Published online: 04 February 2020

REFERENCES

1. Elia, G. A. et al. An overview and future perspectives of aluminum batteries. *Adv. Mater.* **28**, 7564–7579 (2016).
2. Al Sadat, W. I. & Archer, L. A. The O_2-assisted Al/CO_2 electrochemical cell: a system for CO_2 capture/conversion and electric power generation. *Sci. Adv.* **2**, e1600968 (2016).
3. Yang, H. et al. An aluminum–sulfur battery with a fast kinetic response. *Angew. Chem. Int. Ed.* **57**, 1898–1902 (2018).
4. Yu, X. & Manthiram, A. Electrochemical energy storage with a reversible nonaqueous room-temperature aluminum–sulfur chemistry. *Adv. Energy Mater.* **7**, 1700561 (2017).
5. Flahaut, J. A variety of aluminum sulfide stable at high temperature. *Compt. Rend.* **232**, 2100–2102 (1951).
6. Flahaut, J. *Contribution à l'étude du sulfure d'aluminium et des thioaluminates: Jean Flahaut;[Mit 17 Tab. u. 2 Abb.]*, Masson (1952).
7. Krebs, B., Schiemann, A. & Läge, M. Synthese und Kristallstruktur einer Neuen hexagonalen Modifikation von Al_2S_3 mit fünffach koordiniertem Aluminium. *Z. Anorg. Allg. Chem.* **619**, 983–988 (1993).
8. Amaresh, S., Karthikeyan, K., Kim, K. J., Lee, Y. G. & Lee, Y. S. Aluminum based sulfide solid lithium ionic conductors for all solid state batteries. *Nanoscale* **6**, 6661–6667 (2014).
9. Chu, W. et al. A low-cost deep eutectic solvent electrolyte for rechargeable aluminum-sulfur battery. *Energy Storage Mater.* **22**, 418–423 (2019).
10. Flahaut, J. Sur La Preparation Et La Structure Cristalline Du Sulfure Daluminium S_3Al_2. *C. R. Hebd. Seances Acad. Sci.* **232**, 334–336 (1951).
11. Donohue, P. C. High-pressure spinel type Al_2S_3 and $MnAl_2S_4$. *J. Solid State Chem.* **2**, 6–8 (1970).
12. Kvashnin, A. G., Kruglov, I. A., Semenok, D. V. & Oganov, A. R. Iron superhydrides FeH_5 and FeH_6: stability, electronic properties, and superconductivity. *J. Phys. Chem. C.* **122**, 4731–4736 (2018).
13. Majumdar, A., Tse, J. S., Wu, M. & Yao, Y. Superconductivity in FeH_5. *Phys. Rev. B* **96**, 201107 (2017).
14. Pepin, C. M., Geneste, G., Dewaele, A., Mezouar, M. & Loubeyre, P. Synthesis of FeH_5: A layered structure with atomic hydrogen slabs. *Science* **357**, 382 (2017).
15. Yan, X. et al. High-temperature- and high-pressure-induced formation of the Laves-phase compound XeS_2. *Phys. Rev. B* **93**, 214112 (2016).
16. Yang, G., Wang, Y., Peng, F., Bergara, A. & Ma, Y. Gold as a 6p-element in dense lithium aurides. *J. Am. Chem. Soc.* **138**, 4046–4052 (2016).
17. Zhao, Z. et al. Predicted pressure-induced superconducting transition in electride Li_6P. *Phys. Rev. Lett.* **122**, 097002 (2019).
18. Duan, D. et al. Pressure-induced decomposition of solid hydrogen sulfide. *Phys. Rev. B* **91**, 180502 (2015).
19. Li, Y., Hao, J., Liu, H., Li, Y. & Ma, Y. The metallization and superconductivity of dense hydrogen sulfide. *J. Chem. Phys.* **140**, 174712 (2014).
20. Drozdov, A. P., Eremets, M. I., Troyan, I. A., Ksenofontov, V. & Shylin, S. I. Conventional superconductivity at 203 kelvin at high pressures in the sulfur hydride system. *Nature* **525**, 73 (2015).
21. Kokail, C., Heil, C. & Boeri, L. Search for high-T_c conventional superconductivity at megabar pressures in the lithium-sulfur system. *Phys. Rev. B* **94**, 060502 (2016).
22. Feng, X. et al. High-pressure modulated structures in beryllium chalcogenides. *Phys. Rev. B* **100**, 014102 (2019).
23. Wang, Y., Lv, J., Zhu, L. & Ma, Y. Crystal structure prediction via particle-swarm optimization. *Phys. Rev. B* **82**, 094116 (2010).
24. Wang, Y., Lv, J., Zhu, L. & Ma, Y. CALYPSO: a method for crystal structure prediction. *Comput. Phys. Commun.* 183, (2063–2070 (2012).
25. Kresse, G. & Furthmüller, J. Efficient iterative schemes for ab initio total-energy calculations using a plane-wave basis set. *Phys. Rev. B* **54**, 11169–11186 (1996).
26. Becke, A. D. & Edgecombe, K. E. A simple measure of electron localization in atomic and molecular systems. *J. Chem. Phys.* **92**, 5397–5403 (1990).
27. Maintz, S., Deringer, V. L., Tchougréeff, A. L. & Dronskowski, R. Analytic projection from plane-wave and PAW wavefunctions and application to chemical-bonding analysis in solids. *J. Comput. Chem.* **34**, 2557–2567 (2013).
28. Deringer, V. L., Tchougréeff, A. L. & Dronskowski, R. Crystal orbital hamilton population (COHP) analysis as projected from plane-wave basis sets. *J. Phys. Chem. A* **115**, 5461–5466 (2011).
29. Shelton, R. N., Moodenbaugh, A. R., Dernier, P. D. & Matthias, B. T. The effect of pressure on the superconducting and crystallographic transitions of La_3S_4, La_3Se_4 and La_3Te_4. *Mater. Res. Bull.* **10**, 1111–1119 (1975).
30. Oh, J. S. et al. Evidence for anionic excess electrons in a quasi-two-dimensional Ca_2N electride by angle-resolved photoemission spectroscopy. *J. Am. Chem. Soc.* **138**, 2496–2499 (2016).
31. Ming, W., Yoon, M., Du, M.-H., Lee, K. & Kim, S. W. First-principles prediction of thermodynamically stable two-dimensional electrides. *J. Am. Chem. Soc.* **138**, 15336–15344 (2016).
32. Lee, K., Kim, S. W., Toda, Y., Matsuishi, S. & Hosono, H. J. N. Dicalcium nitride as a two-dimensional electride with an anionic electron layer. *Nature* **494**, 336 (2013).
33. Henkelman, G., Arnaldsson, A. & Jónsson, H. A fast and robust algorithm for Bader decomposition of charge density. *Comp. Mater. Sci.* **36**, 354–360 (2006).
34. Miao, M.-s et al. Anionic chemistry of noble gases: formation of Mg–NG (NG = Xe, Kr, Ar) compounds under pressure. *J. Am. Chem. Soc.* **137**, 14122–14128 (2015).
35. Miao, M.-S. & Hoffmann, R. High pressure electrides: a predictive chemical and physical theory. *Acc. Chem. Res.* **47**, 1311–1317 (2014).
36. Miao, M.-s & Hoffmann, R. High-pressure electrides: the chemical nature of interstitial quasiatoms. *J. Am. Chem. Soc.* **137**, 3631–3637 (2015).
37. Tsuji, Y., Dasari, P. L. V. K., Elatresh, S. F., Hoffmann, R. & Ashcroft, N. W. Structural diversity and electron confinement in Li_4N: potential for 0-D, 2-D, and 3-D electrides. *J. Am. Chem. Soc.* **138**, 14108–14120 (2016).
38. Wang, J. et al. Exploration of stable strontium phosphide-based electrides: theoretical structure prediction and experimental validation. *J. Am. Chem. Soc.* **139**, 15668–15680 (2017).
39. Inoshita, T., Jeong, S., Hamada, N. & Hosono, H. Exploration for two-dimensional electrides via database screening and ab initio calculation. *Phys. Rev. X* **4**, 031023 (2014).
40. Pickard, C. J. & Needs, R. Aluminium at terapascal pressures. *Nat. Mater.* **9**, 624 (2010).
41. Ma, Y. et al. Transparent dense sodium. *Nature* **458**, 182 (2009).
42. Li, P., Gao, G., Wang, Y. & Ma, Y. Crystal structures and exotic behavior of magnesium under pressure. *J. Phys. Chem. C.* **114**, 21745–21749 (2010).

43. Matsuishi, S. et al. Direct synthesis of powdery inorganic electride $[Ca_{24}Al_{28}O_{64}]^{4+}(e^-)_4$ and determination of oxygen stoichiometry. *Chem. Mater.* **21**, 2589–2591 (2009).
44. Burton, L. A., Ricci, F., Chen, W., Rignanese, G.-M. & Hautier, G. High-throughput identification of electrides from all known inorganic materials. *Chem. Mater.* **30**, 7521–7526 (2018).
45. Zhang, Y., Wu, W., Wang, Y., Yang, S. A. & Ma, Y. Pressure-stabilized semiconducting electrides in alkaline-earth-metal subnitrides. *J. Am. Chem. Soc.* **139**, 13798–13803 (2017).
46. Miao, M.-s Caesium in high oxidation states and as a p-block element. *Nat. Chem.* **5**, 846 (2013).
47. Hohenberg, P. & Kohn, W. Elementary excitations in solids. *Phys. Rev.* **136**, B864–B871 (1964).
48. Kohn, W. & Sham, L. J. Self-consistent equations including exchange and correlation effects. *Phys. Rev.* **140**, A1133 (1965).
49. Perdew, J. P. et al. Erratum: Atoms, molecules, solids, and surfaces: applications of the generalized gradient approximation for exchange and correlation. *Phys. Rev. B* **48**, 4978–4978 (1993).
50. Blöchl, P. E. Projector augmented-wave method. *Phys. Rev. B* **50**, 17953–17979 (1994).
51. Togo, A., Oba, F. & Tanaka, I. First-principles calculations of the ferroelastic transition between rutile-type and $CaCl_2$-type SiO_2 at high pressures. *Phys. Rev. B* **78**, 134106 (2008).
52. Maintz, S., Deringer, V. L., Tchougréeff, A. L. & Dronskowski, R. LOBSTER: a tool to extract chemical bonding from plane-wave based DFT. *J. Comput. Chem.* **37**, 1030–1035 (2016).
53. Paolo, G. et al. QUANTUM ESPRESSO: a modular and open-source software project for quantum simulations of materials. *J. Phys. Condens. Mat.* **21**, 395502 (2009).

ACKNOWLEDGEMENTS

The authors would like to acknowledge funding support received from the National Key Research and Development Program of China under Grant Nos. 2016YFB0201200, 2016YFB0201201, and 2016YFB0201204; the National Natural Science Foundation of China under Grant Nos. 11822404, 11974134, 11774127, and 11534003; the Program for JLU Science and Technology Innovative Research Team (JLUSTIRT); the Science Challenge Project No. TZ2016001. Parts of the calculation were performed at the high-performance computing center of Jilin University and at Tianhe2-JK at the Beijing Computational Science Research Center.

AUTHOR CONTRIBUTIONS

Y.M., Y.W. and J.L. conceived the research; S.S. performed the simulations and analyzed the data with the help of W.Z.; S.S. wrote the paper; Y.C., Y.W., J.L. and Y.M. helped to revise the paper. All authors discussed and commented on the paper.

COMPETING INTERESTS

The authors declare no competing interests.

ADDITIONAL INFORMATION

Supplementary information is available for this paper at https://doi.org/10.1038/s41524-020-0278-9.

Correspondence and requests for materials should be addressed to J.L. or Y.W.

Reprints and permission information is available at http://www.nature.com/reprints

Publisher's note Springer Nature remains neutral with regard to jurisdictional claims in published maps and institutional affiliations.